Article

Femtosecond Laser Ablation-ICP-Mass Spectrometry and CHNS Elemental Analyzer Reveal Trace Element Characteristics of Danburite from Mexico, Tanzania, and Vietnam

Le Thi-Thu Huong [1,*] iD **, Laura M. Otter** [2,3,*] iD **, Michael W. Förster** [3],
Christoph A. Hauzenberger [1] **, Kurt Krenn** [1] **, Olivier Alard** [3,4] **, Dorothea S. Macholdt** [2] **,
Ulrike Weis** [2] **, Brigitte Stoll** [2] **and Klaus Peter Jochum** [2] iD

[1] NAWI Graz Geocentre, University of Graz, 8010 Graz, Austria;
christoph.hauzenberger@uni-graz.at (C.A.H.); kurt.krenn@uni-graz.at (K.K.)
[2] Climate Geochemistry Department, Max Planck Institute for Chemistry, 55128 Mainz, Germany;
d.macholdt@mpic.de (D.S.M.); ulrike.weis@mpic.de (U.W.); Brigitte.stoll@mpic.de (B.S.);
k.jochum@mpic.de (K.P.J.)
[3] Department of Earth and Planetary Sciences, Macquarie University, Sydney NSW 2109, Australia;
michael.forster@hdr.mq.edu.au (M.W.F.); olivier.alard@mq.edu.au (O.A.)
[4] Géosciences Montpellier, UMR 5243, CNRS & Université Montpellier, 34095 Montpellier, France
* Correspondence: thi.le@uni-graz.at (L.T.-T.H.); laura.otter@hdr.mq.edu.au (L.M.O.)

check for updates

Abstract: Danburite is a calcium borosilicate that forms within the transition zones of metacarbonates and pegmatites as a late magmatic accessory mineral. We present here trace element contents obtained by femtosecond laser ablation-inductively coupled plasma (ICP)-mass spectrometry for danburite from Mexico, Tanzania, and Vietnam. The Tanzanian and Vietnamese samples show high concentrations of rare earth elements ($\sum$REEs 1900 $\mu g \cdot g^{-1}$ and 1100 $\mu g \cdot g^{-1}$, respectively), whereas Mexican samples are depleted in REEs (<1.1 $\mu g \cdot g^{-1}$). Other traces include Al, Sr, and Be, with Al and Sr dominating in Mexican samples (325 and 1611 $\mu g \cdot g^{-1}$, respectively). Volatile elements, analyzed using a CHNS elemental analyzer, reach <3000 $\mu g \cdot g^{-1}$. Sr and Al are incorporated following $Ca^{2+} = Sr^{2+}$ and $2 B^{3+} + 3 O^{2-} = Al^{3+} + 3 OH^- + \square$ (vacancy). REEs replace Ca^{2+} with a coupled substitution of B^{3+} by Be^{2+}. Cerium is assumed to be present as Ce^{4+} in Tanzanian samples based on the observed Be/REE molar ratio of 1.5:1 following $2 Ca^{2+} + 3 B^{3+} = Ce^{4+} + REE^{3+} + 3 Be^{2+}$. In Vietnamese samples, Ce is present as Ce^{3+} seen in a Be/REE molar ratio of 1:1, indicating a substitution of $Ca^{2+} + B^{3+} = REE^{3+} + Be^{2+}$. Our results imply that the trace elements of danburite reflect different involvement of metacarbonates and pegmatites among the different locations.

Keywords: danburite; trace elements; REE; femtosecond LA-ICP-MS; CHNS elemental analyzer; pegmatites; skarn

1. Introduction

Danburite crystallizes in the orthorhombic system and has the formula $CaB_2Si_2O_8$. Its structure consists of a tetrahedral framework with boron and silicon orderly distributed in different tetrahedral sites. The framework of corner-sharing Si_2O_7 and B_2O_7 groups are interconnected by Ca atoms [1,2]. According to previous studies [3,4], the structural unit of danburite contains two tetrahedrally coordinated cations (T1: B and T2: Si), one calcium, and five oxygen atoms, among which O1, O2, and O3 are bonded to both B and Si, while O4 and O5 are bridging oxygens of the Si_2O_7 and B_2O_7 groups, respectively.

Danburite is one of the few boron minerals that are valued as gemstones. After its discovery in Danbury, Connecticut, USA, colorless gem-quality danburite has been subsequently found in Japan, Mexico, Russia, Sri Lanka, and Switzerland [5]. Exceptionally rare is yellow danburite, which so far has been reportedly found only in Madagascar, Tanzania, Myanmar, and Vietnam [6,7]. The important geological environments that are known to have produced gem-quality danburite specimens include pegmatites and metacarbonates associated with hydrothermal activity [8–10].

Previous studies presenting danburite compositions were generally limited to its major element geochemistry (e.g., [11,12]) due to the lack of microanalytical reference materials for boron minerals. While Huong et al. [7] overcame this issue by applying femtosecond laser ablation-inductively coupled plasma-mass spectrometry (LA-ICP-MS), which allows virtually matrix-independent calibration, their study was confined to a regional scale. Here, we present state-of-the-art femtosecond LA-ICP-MS determination of major and trace element concentrations in danburite from three distinct worldwide distributed occurrences (Tanzania, Vietnam, and Mexico). The aims of this study are (1) to investigate the geochemical differences of danburites from different locations (Tanzania, Vietnam, and Mexico) and rock types (pegmatites and skarn), (2) to elucidate their potential for further provenance discrimination, and (3) to understand the incorporation of trace elements into the danburite structure.

2. Materials and Methods

2.1. Sample Material

For this study, we selected 6 danburite samples from 3 deposits in Mexico, Tanzania, and Vietnam (2 samples from each deposit), representing different geological environments. The Mexican danburites were collected from the polymetallic skarn deposit (sulfides of Ag, Pb, Cu, and Zn) in the Charcas mining district, San Luis Potosi. The area is characterized by marine siliciclastic and volcaniclastic rocks, with 2 domains (east and west) separated by a regional fault [9]. In the region of San Luis Potosí, numerous volcanic systems and igneous rocks are associated with different mineral deposits. The Charcas deposit has a large Ca–B metasomatic envelope composed of early datolite and later danburite. Other minerals associated with danburite include calcite, apophyllite, stilbite, chalcopyrite, sphalerite, and citrine. The samples appear as colorless, transparent, prismatic euhedral crystals and are up to 6 cm in length.

The Tanzanian danburite originates from the central zone of a pegmatite mostly as yellowish, fine-grained, massive, opaque aggregates, but occasionally also as larger single crystals with color and transparency. The mine is referred to by the locals as "Munaraima" and is situated in Eastern Tanzania, at the edge of the Uluguru Mountains [10] near the village of Kivuma. The region around Kivuma is dominated by a metasedimentary sequence including metapelites, gneisses, and spinel and ruby-bearing marbles, which underwent granulite facies metamorphism during the East African Orogen at ~640 Ma [13,14]. Tonalitic dikes and pegmatites, commonly found in this area, intruded the basement rocks during slow cooling of the whole area. The contact zone of marble and pegmatite is dominated by a mineral assemblage consisting of microcline (variety amazonite), blue quartz, kyanite, and dravite, while the core complex is mainly composed of massive quartz and schörl [10]. For this study, small, anhedral, transparent yellow danburite crystals ranging from 0.5 to 1 cm in size were selected.

The Vietnamese danburite samples (1–1.5 cm) appear as yellow, transparent, broken, and slightly rounded crystals and have been found in a placer deposit (Bai Cat) in the Luc Yen mining area, Yen Bai province, Northern Vietnam [7,15]. The geology of Luc Yen is dominated by metamorphic rocks, mainly granulitic gneisses, mica schists, and marbles, which are associated with the large-scale Ailao Shan–Red River shear zone. Locally, aplitic and pegmatitic dykes occur [16]. Danburite crystals are associated with ruby, sapphire, spinel, topaz, and tourmaline in the Bai Cat placer deposit, which is surrounded by marble units. While the primary formations of ruby, sapphire, and spinel in Luc Yen are associated with metamorphosed limestones, those of tourmaline and topaz originate from pegmatite

bodies. Besides tourmaline and topaz, these pegmatites contain orthoclase, smoky quartz, lepidolite, and beryl. Danburite crystals have not yet been discovered in situ, hence their genetic relationship with the Luc Yen pegmatites is not verified. However, fluid inclusion studies of Luc Yen danburites indicate a pegmatitic origin [15].

2.2. Analytical Methods

Chemical data for major elements were obtained by electron microprobe at the Institute of Geosciences, Johannes Gutenberg University Mainz, by laser ablation-inductively coupled plasma-mass spectrometry (LA-ICP-MS) at the Max Planck Institute for Chemistry, Mainz, and by CHNS Elemental Analyzer at Macquarie University.

Electron probe micro-analysis (EPMA) was performed at the University of Mainz with a JEOL JXA 8200 Superprobe instrument equipped with 5 wavelength-dispersive spectrometers, using 15 kV acceleration voltage and 12 nA filament current. Calcium and silicon were analyzed with wollastonite as a standard material.

LA-ICP-MS data for a total of 55 elements were obtained using an NWRFemto femtosecond laser operating at a wavelength of 200 nm in combination with a ThermoFisher Element2 single-collector sector-field ICP mass spectrometer (see Table 1). Pre-ablation cleaning was performed using a spot size of 65 µm, 80 µm/s scan speed, and 50 Hz pulse repetition rate at 100% energy output to remove any superficial surface residue. Thereafter, samples were ablated using line scans of 300 µm length at a spot size of 55 µm and a scan speed of 5 µm/s. These parameters resulted in an energy density of ca. 0.51 J/cm^2 at the sample surface, and the pulse repetition rate was set to 50 Hz. Since there is no matrix-matched calibration material for Ca–B silicates available, we applied a laser device that produces pulses at 150 fs, enabling virtually matrix-independent calibration [17]. The glass microanalytical reference material NIST SRM 610 was used as calibration material in the evaluation process, where ^{43}Ca was used as internal standard. Reduction of data and elimination of obvious outliers were performed following a programmed routine in Microsoft Excel described in Jochum et al. [18].

All samples were additionally analyzed for their H, C, N, and S contents in a vario EL cube elemental analyzer (Elementar, Langenselbold, Germany). For analysis, 50 to 100 mg samples were packed in Sn-foils (no flux added) and were ignited in an oxygen–He gas atmosphere furnace at around 1150 °C. The produced gases were then trapped and released in a set of chromatographic columns for the sequential analysis of N (no trapping), then C, H, and S. Each sample was measured for 9 min, and released gases were sequentially analyzed with a thermal conductivity detector. Sample measurements were repeated 3 times for each sampling location, and all values were calibrated against the reference materials BAM-U110, JP-1, and CRPG BE-N (Table 2). Analytical uncertainties were evaluated from reference material values, which were found to lie within 16% and 25% for C and H of the data tabulated in the GeoReM database [19].

Table 1. Operating conditions of the femtosecond laser ablation-inductively coupled plasma-mass spectrometry (fs-LA-ICP-MS) system.

Operating Conditions of NWRFemto200 Laser System	
Wavelength λ (nm)	200
Fluence (J·cm^{-2})	0.51
Pulse length (fs)	150
Pulse repetition rate (Hz)	50
Laser energy output (%)	100
Spot size (µm)	55
Line length (µm)	300
Scan speed (µm·s^{-1})	5
Warm-up time (s)	28
Dwell time (s)	60
Washout time (s)	30

Table 1. *Cont.*

Operating Conditions of the Element2 Mass Spectrometer	
RF power (W)	1055
Cooling gas (Ar) flow rate (L·min^{-1})	16
Auxiliary gas (Ar) flow rate (L·min^{-1})	1.19
Additional gas (He) flow rate (L·min^{-1})	0.7
Sample gas (Ar) flow rate (L·min^{-1})	0.7
Sample time (s)	0.002
Samples per peak	100
Mass window (%)	10
Time per pass (s)	2
Scan mode (Escan/Bscan)	both
Mass resolution	300

Table 2. Reference materials for CHNS analyzer.

BE-N Altered Basalts (SARM)	H TCD	C TCD	N TCD	S TCD	S IR
n	14	20	17	21	8
Average (µg·g^{-1})	2771 ± 534	2301 ± 147	197 ± 42	301 ± 37	298 ± 23
RSD %	19	6	21	12	8
BAM-U110					
n	13	18	18	17	–
Average (µg·g^{-1})	12,258 ± 1758	72,340 ± 2640	4237 ± 165	9114 ± 1082	–
RSD %	14	4	4	12	–
JP-1 Peridotite massif (JGS)					
n	4	12	14	14	14
Average (µg·g^{-1})	3195 ± 170	763 ± 82	91 ± 23	27 ± 14	26 ± 7
RSD %	5	11	26	51	27

n denotes the number of measurement performed; average refers to arithmetic means of the *n* values measured; RSD % is relative standard deviation expressed in %. "TCD" refers to the thermal conductivity detector and "IR" to the infrared detector devices.

3. Results

The chemical composition of the danburite samples from Mexico, Tanzania, and Vietnam are presented in Table 3. The major element mass fractions of B, Ca, and Si are close to the stoichiometric composition, i.e., 28.32 wt % B_2O_3 (calculated from 87,890 ppm B obtained by ICP-MS), 22.81 wt % CaO, and 48.88 wt % SiO_2, respectively.

The trace elements Li, Sc, Ga, Se, Rb, Zr, Nb, Ag, Cd, Sn, Cs, Hf, Ta, W, Ir, Pt, Au, Tl, Bi, and U have concentrations below the detection limit in all samples (see detection limits in footnote of Table 3). A C1-chondrite–normalized plot of rare earth element (REE) mass fractions (normalizing data from [20]) displays a strong enrichment of light rare earth elements (LREEs: La, Ce, Pr, Nd, Sm, Eu) compared to heavy rare earth elements (HREEs: Gd, Tb, Dy, Ho, Er, Tm, Yb, Lu) in danburite from Tanzania and Vietnam, while the samples from Mexico are mostly below detectability (Figure 1). Europium shows a negative anomaly of the same order for samples from Tanzania and Vietnam, while no other strong anomaly is observed (e.g., Ce). Total lanthanide content of Tanzanian samples is up to 1900 µg·g^{-1}, hence the mass fractions of LREE exceed those of HREE by a 500-fold enrichment. The Vietnamese samples are different, with a total REE content of around 1000 µg·g^{-1}, hence the mass fractions of LREE exceed those of HREE by a 200-fold enrichment. The Mexican danburites appear to be REE-poor, with total REE contents below 1 µg·g^{-1} for La and Ce, while the remaining REEs from Nd to Lu are below the detection limits. Possible quadrivalent trace elements such as Ti, Hf, and Zr were also below the detection limits. Thorium and Pb show low mass fractions of 0.1 and 11 µg·g^{-1} in the Mexican danburites, and 0.6 and 8 µg·g^{-1} in the Vietnamese and Tanzanian danburites, respectively.

The trivalent element Al shows highly varying concentrations among the different deposits and is anti-correlated with $\sum$REE, thus also with Be (see Figure 2A,B), while no correlation was observed between Al and Sr (Figure 2C). The highest mass fractions of Al are found in the Mexican samples (325 $\mu g \cdot g^{-1}$) and the lowest in the Tanzanian samples (84 $\mu g \cdot g^{-1}$) (Table 3). Strontium is highest (1611 $\mu g \cdot g^{-1}$) in the Mexican samples and lowest (66 $\mu g \cdot g^{-1}$) in the Vietnamese samples (Figure 2D). Manganese yields up to 18 $\mu g \cdot g^{-1}$ in the Vietnamese danburites, while the Mexican and Tanzanian samples have Mn contents below the detection limits. In general, transition metals (e.g., Fe and Ni) have extremely low concentrations in all danburite samples. The three danburite origins can also be separated from each other using the mass fractions of Y (Figure 2E). Beryllium is found to be highest in the Tanzanian danburite (up to 178 $\mu g \cdot g^{-1}$) and lowest in the Mexican samples (3 $\mu g \cdot g^{-1}$). In addition, low concentrations of less than 1, 9, and 2 $\mu g \cdot g^{-1}$ of the elements Ba, Mg, and Cu, respectively, are identified in all samples regardless of their origin. The positive correlation between Be and $\sum$REE is exceptionally strong for all three deposits (Figure 3A), and due to varying mass fractions of all shown elements, this plot enables excellent discrimination among the three deposits. Univalent elements such as Li, Na, and, K fall below the detection limits.
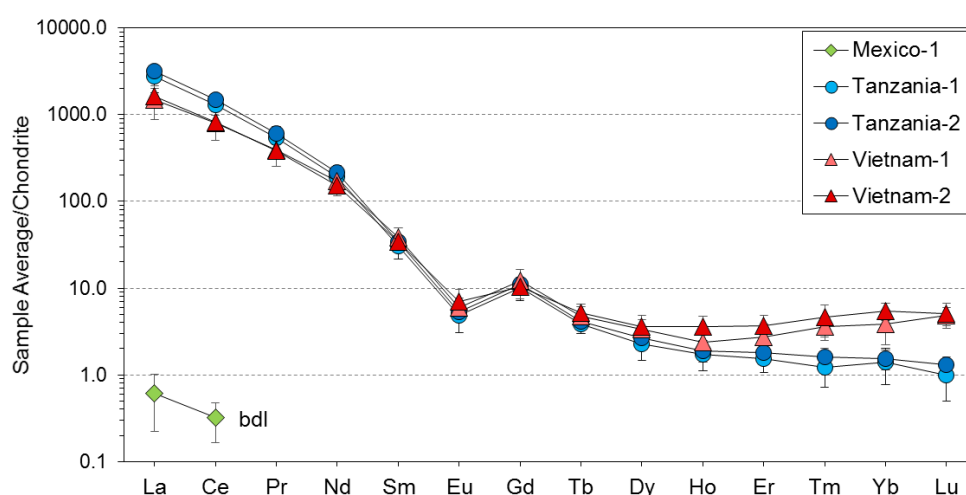

Figure 1. Rare earth element (REE) mass fractions in danburite from Mexico, Tanzania, and Vietnam. All values are presented as averages and normalized to C1-chondrite (data from [20]). Samples from Tanzania and Vietnam have a high abundance of REEs, especially LREEs, while samples from Mexico are largely devoid of these elements (bdl, below detection limit, from Pr to Lu).

The contents of the light volatile elements H, C, N, and S are generally low for both unpowdered and powdered samples (see Table 4). Samples from both Tanzania and Mexico exhibit mass fractions of H, C, N, and S of <10, <200, <100, and <15 $\mu g \cdot g^{-1}$, respectively. The samples from Vietnam show significantly higher mass fractions for H, C, N, and S in unpowdered specimens, reaching values of up to 300, 5600, 1000, and 15 $\mu g \cdot g^{-1}$, respectively. However, most elements are present in lower concentrations in the powdered sample set (H, C, and N of 40, 3000, and 520 $\mu g \cdot g^{-1}$, respectively). Higher values for powdered samples from Mexico and Tanzania are likely attributed to the significantly increased surface-to-volume ratio facilitating higher adhesion of atmospheric gases. Significantly higher values for H and C in all Vietnamese samples agree well with a previous study by Huong et al. [15], who characterized a high abundance of primary CO_2-bearing fluid inclusions in these samples, which likely accounts for the elevated concentrations of both elements, while fluid inclusion is not present in the Mexican or Tanzanian specimens. High N mass fractions are in the expected range of metamorphosed sediments, which are involved in danburite formation and are known to contain ~200–3000 $\mu g \cdot g^{-1}$ N for a typical metamorphic gradient of 500–700 °C (e.g., [21]). Overall lower values of H, C, and N in the powdered Vietnamese sample set support the observation

that these elements are derived from fluid inclusions and were lost during crushing in the agate mortar. Nevertheless, powdered samples were still found to contain up to 40 µg·g^{-1} structurally bound H (equivalent to 0.036 wt % H_2O+), which is close to the value of 0.04 wt % H_2O+ determined by IR spectroscopy as published in [4].
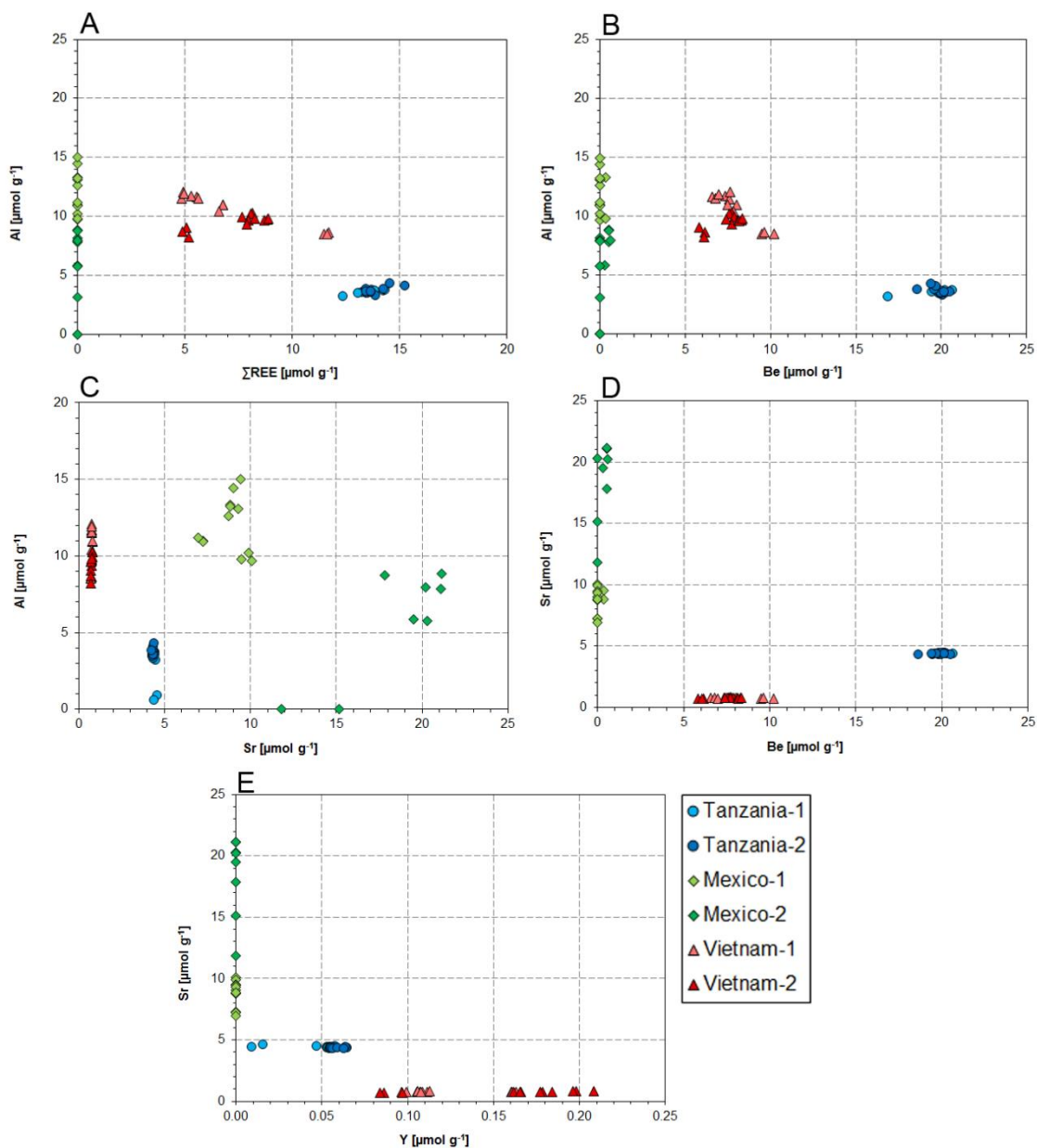

Figure 2. Molar abundance of Al versus (**A**) ∑REE, (**B**) Be, and (**C**) Sr, and Sr versus (**D**) Be and (**E**) Y. Aluminum is negatively correlated with (**A**) REEs, (**B**) Be, and (**D**) partly Sr, while Sr correlates negatively with (**D**) Be and (**E**) Y.
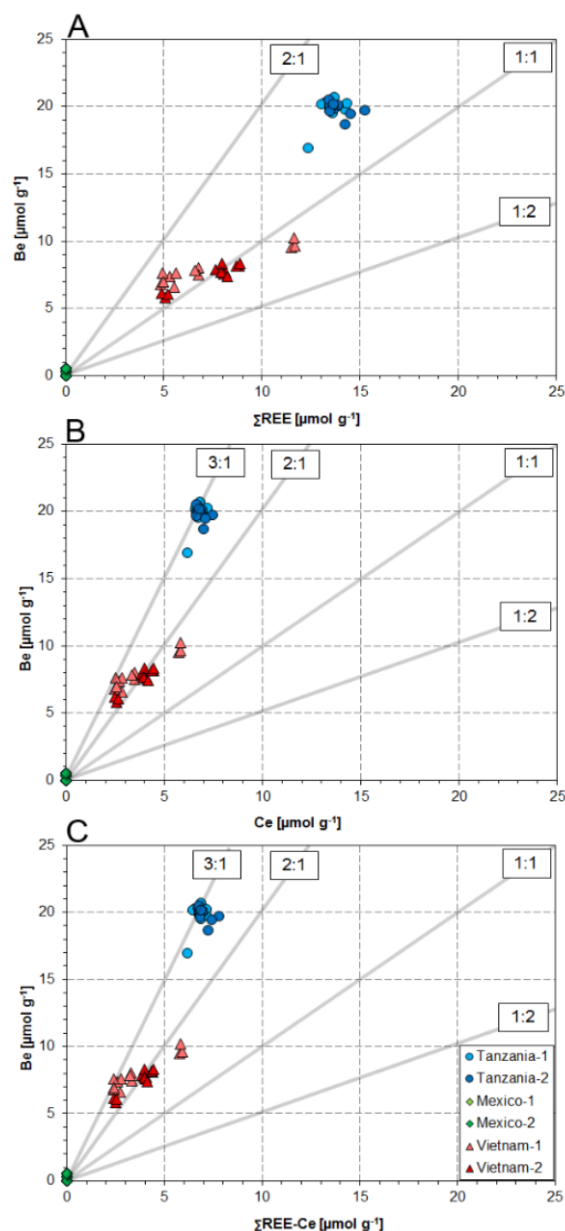
Figure 3. (**A**) Molar abundance of Be shows a linear correlation with $\sum$REE and illustrates that incorporation of REEs in the danburite structure is accompanied by Be. The Be/$\sum$REE ratio in Tanzanian samples is approximately 1.5:1, while it varies in Vietnamese samples from ca. 1:1 to ca. 1.5:1. Correlations between Be and $\sum$REE are ideally suited to distinguish danburite sampling locations. However, the simple substitution equation $Ca^{2+} + B^{3+} = REE^{3+} + Be^{2+}$, where the Be/$\sum$REE ratio is 1:1, is not sufficient to explain the varying ratios of Be and $\sum$REE. (**B**) Molar abundance of Be and Ce shows a linear correlation, implying that incorporation of Ce into the danburite structure is accompanied by Be. The Be/Ce ratio in Tanzanian samples is approx. 3:1, while in Vietnamese samples it varies from ca. 2:1 to ca. 3:1. The equation $2\,Ca^{2+} + 3\,B^{3+} = Ce^{4+} + REE^{3+} + 3\,Be^{2+}$, where the Be/Ce ratio is 3:1, explains the Tanzanian and most of the Vietnamese cases very well. Therefore, we argue here that Ce occurs not only as Ce^{3+}, but also as Ce^{4+} in Tanzanian and Vietnamese danburite and the substitution mechanism $2\,Ca^{2+} + 3\,B^{3+} = Ce^{4+} + REE^{3+} + 3\,Be^{2+}$ takes places in these samples. (**C**) Be/($\sum$REE − Ce) ratios show similar behavior to Be/Ce ratios. As the Be/($\sum$REE − Ce) ratios vary from 2:1 to 3:1, both substitution mechanisms should take place: $Ca^{2+} + B^{3+} = REE^{3+} + Be^{2+}$, $2\,Ca^{2+} + 3\,B^{3+} = Ce^{4+} + REE^{3+} + 3\,Be^{2+}$.

Table 3. Average chemical composition (in µg·g^{-1} and µmol·g^{-1}) and relative standard deviation (RSD, %) obtained from danburite of three different occurrences. All concentrations were obtained by fs LA-ICP-MS (n = 12 line scans), except CaO and SiO$_2$, which were evaluated with Electron Probe Microanalyzer (EPMA) (averaged from n = 20 spot analyses per sample).

| Element | Isotope Used | L.O.D. | Charcas, San Luis Potosi, Mexico | | | | | | Morogoro, Tanzania | | | | | | Luc Yen, Vietnam | | | | | |
| | | | Mex-1 | | | Mex-2 | | | Tanz-1 | | | Tanz-2 | | | Viet-1 | | | Viet-2 | | |
			Ø (µg·g^{-1})	Ø (µmol·g^{-1})	RSD (%)	Ø (µg·g^{-1})	Ø (µmol·g^{-1})	RSD (%)	Ø (µg·g^{-1})	Ø (µmol·g^{-1})	RSD (%)	Ø (µg·g^{-1})	Ø (µmol·g^{-1})	RSD (%)	Ø (µg·g^{-1})	Ø (µmol·g^{-1})	RSD (%)	Ø (µg·g^{-1})	Ø (µmol·g^{-1})	RSD (%)
CaO*	–	–	**22.47**	**0.04**	**0.49**	**22.43**	**–**	**0.71**	**22.63**	**0.04**	**0.60**	**22.48**	**0.04**	**0.57**	**22.32**	**0.03**	**0.51**	**22.40**	**0.03**	**0.37**
B	11	10	86218	7975	6.67	90471	8368	4.05	86280	7981	1.56	87270	8072	2.69	85698	7927	3.13	89138	8245	3.19
SiO$_2$ *	–	–	**48.31**	**0.8**	**0.40**	**48.81**	**0.8**	**0.33**	**48.80**	**0.8**	**0.36**	**48.88**	**0.8**	**0.38**	**48.81**	**0.8**	**0.43**	**48.43**	**0.8**	**0.37**
La	139	0.01	0.15	0.0011	63.5	0.01	0.0001	124.0	675	4.9	35.3	807	5.8	4.7	368	2.7	42.3	400	2.9	22.0
Ce	140	0.01	0.20	0.0014	48.1	0.05	0.0004	10.00	827	5.9	34.7	964	6.9	3.4	508	3.6	36.9	525	3.8	19.6
Pr	141	0.03	<0.03	–	–	<0.03	–	–	51.4	0.37	35.1	59.5	0.42	4.0	37.4	0.27	35.3	36.5	0.26	17.5
Nd	143	0.08	<0.08	–	–	<0.08	–	–	91.1	0.63	34.5	106	0.74	4.9	80.9	0.56	32.2	72.8	0.51	16.2
Sm	147	0.05	<0.05	–	–	<0.05	–	–	4.65	0.03	28.7	5.68	0.04	9.6	5.94	0.04	27.1	5.23	0.03	18.7
Eu	151	0.05	<0.05	–	–	<0.05	–	–	0.28	0.002	37.7	0.31	0.002	14.1	0.34	0.002	28.5	0.41	0.003	38.2
Gd	157	0.04	<0.04	–	–	<0.04	–	–	2.05	0.013	28.1	2.38	0.015	10.9	2.46	0.016	37.1	2.13	0.014	28.3
Tb	159	0.01	<0.01	–	–	<0.01	–	–	0.15	0.001	22.4	0.16	0.001	15.5	0.18	0.001	29.5	0.20	0.001	26.1
Dy	163	0.05	<0.05	–	–	<0.05	–	–	0.58	0.004	35.7	0.68	0.004	7.80	0.85	0.005	30.5	0.92	0.006	33.7
Ho	165	0.01	<0.01	–	–	<0.01	–	–	0.10	0.001	35.9	0.11	0.001	11.3	0.13	0.001	40.3	0.20	0.001	31.1
Er	167	0.04	<0.04	–	–	<0.04	–	–	0.25	0.001	30.0	0.28	0.002	38.6	0.46	0.003	41.0	0.61	0.004	33.3
Tm	169	0.02	<0.02	–	–	<0.02	–	–	0.03	0.0002	40.5	0.04	0.0002	49.3	0.09	0.0005	31.4	0.12	0.0007	40.1
Yb	173	0.04	<0.04	–	–	<0.04	–	–	0.23	0.0013	44.4	0.26	0.0015	32.5	0.64	0.0037	42.1	0.90	0.0052	22.4
Lu	175	0.02	<0.02	–	–	<0.02	–	–	0.02	0.0001	50.3	0.03	0.0002	43.5	0.12	0.0007	23.7	0.13	0.0007	32.2
Al	27	10	325	12.0	14.9	171	6.4	40.5	84.3	3.1	36.2	101	3.7	7.58	288	10.7	12.8	257	9.5	6.41
As	69	1	46.6	0.6	8.74	7.05	0.1	19.0	<1	0.01	56.5	<1	0.01	67.8	1.13	0.02	103	1.10	0.01	46.0
Ba	135, 137	0.1	0.50	0.004	54.1	0.19	0.001	36.60	0.29	0.002	25.06	0.22	0.002	14.77	0.48	0.003	89.66	0.63	0.005	27.03
Be	9	3	3.06	0.3	12.5	4.94	0.5	26.0	156	17.4	32.8	178	19.8	2.42	71.7	8.0	14.09	67.0	7.4	12.2
Cr	53	5	<5	–	–	<5	–	–	<5	–	–	<5	–	–	6.44	0.12	43.8	<5	–	–
Cu	65	1	1.56	0.02	65.3	<1	–	–	<1	–	–	<1	–	–	1.10	0.02	78.2	2.00	0.03	56.4
Fe	57	20	<20	–	–	<20	–	–	<20	–	–	<20	–	–	<20	–	–	<20	–	–
K	39	7	<7	–	–	<7	–	–	<7	–	–	<7	–	–	<7	–	–	<7	–	–
Mg	25	9	<9	–	–	<9	–	–	<9	–	–	<9	–	–	<9	–	–	<9	–	–
Mn	55	1	<1	–	–	<1	–	–	<1	–	–	<1	–	–	18.4	0.34	8.93	14.57	0.27	14.3
Na	23	50	<50	–	–	<50	–	–	<50	–	–	<50	–	–	<50	–	–	<50	–	–
Ni	62	18	<18	–	–	<18	–	–	<18	–	–	<18	–	–	<18	–	–	<18	–	–
Pb	207, 208, 209	0.1	0.27	0.0013	49.2	0.23	0.0011	40.0	7.46	0.0360	33.8	8.05	0.0389	8.94	11.1	0.0534	5.05	10.6	0.0514	5.60

Table 3. *Cont.*

| Element | Isotope Used | L.O.D. | Charcas, San Luis Potosi, Mexico | | | | | | Morogoro, Tanzania | | | | | | Luc Yen, Vietnam | | | | | |
| | | | Mex-1 | | | Mex-2 | | | Tanz-1 | | | Tanz-2 | | | Viet-1 | | | Viet-2 | | |
			Ø (µg·g⁻¹)	Ø (µmol·g⁻¹)	RSD (%)	Ø (µg·g⁻¹)	Ø (µmol·g⁻¹)	RSD (%)	Ø (µg·g⁻¹)	Ø (µmol·g⁻¹)	RSD (%)	Ø (µg·g⁻¹)	Ø (µmol·g⁻¹)	RSD (%)	Ø (µg·g⁻¹)	Ø (µmol·g⁻¹)	RSD (%)	Ø (µg·g⁻¹)	Ø (µmol·g⁻¹)	RSD (%)
Sb	121, 123	1	13.0	0.1	81.9	35.8	0.3	75.6	<1	–	–	<1	–	–	<1	–	–	<1	–	–
Sr	88	0.1	767	8.8	12.09	1611	14.8	40.6	387	4.4	1.44	381	4.4	1.02	66.5	0.8	2.81	66.1	0.8	5.08
Th	232	0.01	<0.01	–	–	<0.01	–	–	0.47	0.0020	41.3	0.66	0.0028	8.45	0.11	0.0005	51.7	0.11	0.0005	44.6
Ti	49	3	<3	–	–	<3	–	–	<3	–	–	<3	–	–	<3	–	–	<3	–	–
V	51	0.5	0.71	0.01	36.54	0.98	0.02	19.1	0.84	0.02	10.8	0.83	0.02	11.3	0.73	0.01	33.8	0.95	0.02	22.5
Y	89	0.1	<0.1	–	–	<0.1	–	–	4.21	0.05	35.1	5.23	0.1	6.19	10.6	0.1	21.2	14.1	0.2	27.9
Zn	67	10	59.6	0.9	34.6	27.5	0.4	53.1	15.8	0.2	32.5	15.5	0.2	41.7	63.2	1.0	39.3	89.9	1.4	49.0

* (wt %), excluded due to concentrations below limits of detection (L.O.D.) in µg·g⁻¹ in all samples: Li (<5), Sc (<1), Ga (<0.5), Se (<10), Rb (<0.5), Zr (<0.1), Nb (<0.01), Ag (<0.1), Cd (<1), Sn (<1), Cs (<0.1), Hf (<0.01), Ta (<0.01), W (<0.01), Ir (<0.01), Pt (<0.01), Au (<0.1), Tl (<0.1), Bi (<0.01), and U (<0.01).

Table 4. Light volatile elements in unpowdered and powdered danburite samples provided as $\mu g \cdot g^{-1}$; calculated H_2O+ values are given in wt %.

Sample Location	Unpowdered Samples					Powdered Samples				
	H	eq. H_2O+ (wt %)	C	N	S	H	eq. H_2O+ (wt %)	C	N	S
Mexico	<10	<0.01	200 ± 5	50 ± 10	13 ± 1	31 ± 10	0.028	130 ± 50	230 ± 130	25 ± 7
Tanzania	<10	<0.01	120 ± 40	100 ± 50	8 ± 1	14 ± 1	0.012	70 ± 40	100 ± 50	22 ± 3
Vietnam	300 ± 50	0.244	5600 ± 20	1000 ± 10	15 ± 3	40 ± 10	0.036	3000 ± 40	520 ± 20	19 ± 11

4. Discussion

4.1. Substitution Mechanisms of REEs, Be, and Sr in Danburite Structure

Referring to the similarity in ionic size and charge, eightfold-coordinated Ca^{2+} (1.12 Å) can be replaced to a certain extent by Sr^{2+} (1.26 Å). This substitution commonly takes place in danburite from all deposits and is mostly observed in the Mexican samples, where the concentration of Sr reaches 1611 $\mu g \cdot g^{-1}$, followed by the Tanzanian and Vietnamese samples, with Sr concentrations up to 387 $\mu g \cdot g^{-1}$ and 66 $\mu g \cdot g^{-1}$, respectively (Table 3).

$$Ca^{2+} = Sr^{2+} \tag{1}$$

Another substitution in danburite is the replacement of Ca^{2+} by REE^{3+} (here we presume that all REEs are trivalent, with the exception of Ce, which can be quadrivalent under strongly oxidizing conditions). It is obvious that danburite from all deposits prefer to incorporate LREE over HREE by a 200- to 500-fold enrichment. The REE^{3+} have decreasing radii with respect to increasing atomic number, i.e., from La (1.16 Å) to Ce (1.15 Å) to Lu (0.98 Å). Moreover, LREE radii are more compatible with the eightfold-coordinated Ca^{2+} lattice site. This explains why LREEs, especially La and Ce, are preferentially incorporated in the danburite lattice. The negative Eu anomaly observed in the Vietnamese and Tanzanian danburite is in accordance with a general depletion of Eu in highly oxidized magma, such as granites and pegmatites [22].

The substitution of Ca^{2+} by a REE^{3+} requires charge compensation and is therefore coupled with the substitution of B^{3+} (0.11 Å) by Be^{2+} (0.27 Å) and/or Si^{4+} (0.26 Å) by Al^{3+} (0.39 Å). These coupled substitutions theoretically allow all sites to be filled and charges to be balanced accordingly:

$$Ca^{2+} + B^{3+} = REE^{3+} + Be^{2+} \tag{2}$$

$$Ca^{2+} + Si^{4+} = REE^{3+} + Al^{3+} \tag{3}$$

An omission-style substitution of Ca^{2+} by a trivalent REE^{3+} is also suitable to gain charge balance:

$$3Ca^{2+} = 2REE^{3+} + \square \text{ (vacancy)} \tag{4}$$

However, the positive correlation of molar abundance of REE and Be suggests that Equation (2) is the dominating process of REE incorporation into the danburite lattice (Figure 3A). The remaining substitution Equations (3) and (4) are theoretically possible, but are not supported by the datasets, which show, e.g., a negatively correlated relationship of Al with $\sum$REE (Figure 2A). In the Vietnamese samples, the Be/REE ratio is at an approximate 1:1 trend. In the Tanzanian samples, all the values are approximately equal to 1.5:1 (Figure 3A). A Be/REE ratio that is equal to or higher than 1:1 indicates that REEs are fully coupled with Be; subsequently, the two other forms of substitution, $Ca^{2+} + Si^{4+} = REE^{3+} + Al^{3+}$ (3) and $3Ca^{2+} = 2REE^{3+} + \square$ (4), are subordinate mechanisms. However, Equation (2) implies a Be/REE ratio equal to 1:1, rather than the 1.5:1 ratio measured in the Tanzanian samples. Hence, the excessive molar abundance of Be over REE in the Tanzanian samples needs to be explained by another substitution process with different ratios for Be and REEs or by an REE-independent substitution mechanism. This first hypothesis leads to the suggestion that

Ce occurs not only as Ce^{3+}, but also Ce^{4+} in the samples (with ionic sizes of 1.15 Å and 0.97 Å, respectively). The existence of Ce^{4+} in geological materials has been observed in various studies [23–26]. Hence, we extend substitution mechanism (2) to account for the probable presence of quadrivalent Ce:

$$2Ca^{2+} + 3B^{3+} = Ce^{4+} + REE^{3+} + 3Be^{2+} \tag{5}$$

Equation (5) is an example of a substitution mechanism where the ratio of $\sum$REEs (all REE^{3+} and Ce^{4+}) to Be is equal to 3:2 (or 1.5:1). According to Equation (5), the ratios Be/Ce and Be/($\sum$REEs − Ce) are both 3:1. Our chemical data (Figure 3B,C) show that the Be/Ce and Be/($\sum$REEs − Ce) ratios in the Tanzanian samples are approximately 3:1 and 1.5:1. Therefore, we assume that mechanisms (2) and (5) take place predominantly in the Vietnamese and Tanzanian samples, respectively, with Ce likely present as Ce^{3+} and Ce^{4+}, respectively. This might suggest that REE uptake into Tanzanian danburite occurs at elevated oxygen fugacity compared to Mexican and Vietnamese danburite.

4.2. Substitution Mechanisms Involving OH and Al in the Danburite Lattice

The presence of Be may also be the result of a REE-independent substitution of B^{3+} by Be^{2+} coupled with the substitution of O^{2-} by OH^-:

$$B^{3+} + O^{2-} = Be^{2+} + OH^- \tag{6}$$

The presence of OH^- species in the danburite lattice was indicated in [4,7] by means of FTIR spectroscopy. The bridging oxygen O5 in the B_2O_7 group is an ideal candidate for partial OH^- replacement, which allows the presence of low amounts of OH^- in danburite. However, a coupled incorporation of Be^{2+} and OH^- was not observed in our study (Figure 4A). Beran [4] proposed a coupled 1:1 substitution of Si^{4+} and O^{2-} by Al^{3+} and OH^- to charge balance OH incorporation. However, a direct substitution (1:1) was not confirmed by either dataset in the present study. Instead, we observed a positive correlation of Al^{3+} with OH^- (Figure 4B) in a 1:3 ratio, which suggests a coupled incorporation of Al^{3+} and OH^-, substituting for B^{3+} and O^{2-}, respectively:

$$2B^{3+} + 3O^{2-} = Al^{3+} + 3OH^- + \square \text{ (vacancy)} \tag{7}$$
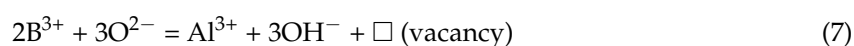
Regarding the possibility of Al incorporation into danburite, it should be noted that the geochemical behavior of B^{3+} and Al^{3+} is very similar; however, they differ in radius size, with 0.11 Å for B^{3+} and 0.39 Å for Al^{3+} when in a tetrahedral coordination environment. Hence, a simple substitution mechanism such as $B^{3+} = Al^{3+}$ would not be possible. Although a substitution of Al^{3+} with B^{3+} has been observed in the system albite $NaAlSi_3O_8$ - $NaBSi_3O_8$ reedmergnerite [27], as well as in a synthetic phlogopite $KMg_3(BSi_3)O_{10}(OH)_2$ [28], this process seems not to be valid for the danburite datasets (Figure 4A,B). Substitution mechanism (7) explains the Mexican samples as well, where the Al concentration is high and both REE and Be concentrations are low.

In general, the four main substitution mechanisms discussed above take place with different priority in the three studied locations. The substitutions of Ca^{2+} by Sr^{2+} and $2B^{3+}$ by Al^{3+} are more common in the Mexican samples, while the substitutions of Ca^{2+} by REEs in the forms $Ca^{2+} + B^{3+} = REE^{3+} + Be^{2+}$ and $2Ca^{2+} + 3B^{3+} = Ce^{4+} + REE^{3+} + 3Be^{2+}$ are more common in the Vietnamese and Tanzanian samples, respectively.
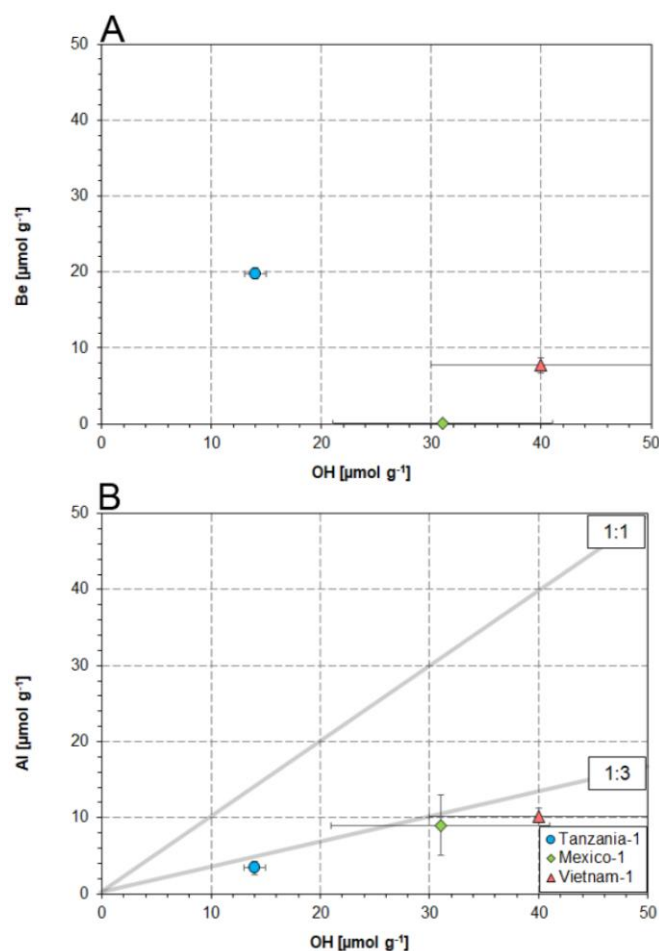
Figure 4. (**A**) Beryllium and OH correlate negatively, which suggests that incorporation into the danburite structure is not coupled. (**B**) However, Al shows a positive correlation with OH at a 1:3 ratio for all sampling locations, making a coupled incorporation of Al with OH likely.

4.3. Constraints on the Geochemical Formation Environment of Danburite

Since danburite samples from Tanzania and Vietnam show a similar strong enrichment in LREE, the reported low values in the Mexican samples must therefore mean either a deficit of REE in the source material or REEs were already sequestered in datolite, which co-occurs with Mexican danburite. However, the depletion of REEs in the Mexican samples is accompanied by exceedingly high amounts of Sr (ca. 1000 $\mu g \cdot g^{-1}$ on average), which is an independent indicator of a different source composition with a higher component of biogenic calcareous sediments in the source material of this location. Biogenic limestone is known to contain high Sr values by being virtually free of REE [29,30]. In comparison, samples from Vietnam and Tanzania exhibit high REE, Y, and Be coupled with low Sr, thereby representing a composition that results from the involvement of highly differentiated late-stage silicic magmas (i.e., pegmatites). This is in agreement with the observed negative Eu anomalies in these samples, which are characteristic for late magmas, where the depletion in Eu is driven by fractional crystallization of plagioclase, which is commonly found to incorporate high amounts of Eu^{2+} [22]. This is in agreement with the nature of the outcrop and mineral assemblage in which the danburite was found. The high compatibility of LREE in the danburite lattice must therefore only be limited by the availability from the source material (i.e., highest in Tanzanian and lowest in Mexican samples). High contents of REE are in accordance with the significantly low amounts of N in the Tanzanian samples, due to the incompatibility of N in highly fractionated magmatic rocks, indicating a strong pegmatite component in the Tanzanian samples. Charge compensation and a

Be/∑REEs ratio of 1.5:1 indicate the presence of Ce^{4+} (Equation (5)), additionally supporting a highly oxidized pegmatitic source for the Tanzanian samples. Nitrogen mass fractions generally increase with decreasing temperature and increasing involvement of metamorphic rocks (e.g., [21]), which suggests that the Vietnamese and Mexican samples were either formed at greater distance from the pegmatite or sourced from a higher proportion of recycled metamorphic rocks. Hence, we conclude that even though danburite always forms in a transition zone of metacarbonates and pegmatites, there are significant geochemical differences, i.e., ∑REE, Be, Sr, Al, and OH in danburite, that directly reflect the different proportions and compositions of these source materials. Thus, our results suggest that trace element concentrations are suitable for determining the origins and locations of danburite crystals (i.e., for gem-testing laboratories).

5. Conclusions

In this study, we investigated trace element variations of danburite from three different locations in Mexico, Tanzania, and Vietnam. The most important trace elements in danburite that reflect their provenance include REEs, Sr, Al, Be, and, to a lesser extent, Mn, Zn, and Y. Mexican samples are fairly devoid of REEs, while Tanzanian samples contain up to 1900 $\mu g \cdot g^{-1}$ and Vietnamese samples have intermediate total values of around 1100 $\mu g \cdot g^{-1}$. LREEs are more abundant than HREEs in all danburite samples, showing a 200- to 500-fold relative enrichment. Strontium and Al are more enriched in Mexican danburite than in Tanzanian and Vietnamese danburite, with mass fractions up to 1611 and 325 $\mu g \cdot g^{-1}$, respectively.

Based on fs-LA-ICP-MS and CHNS analysis, we identified four mechanisms of trace element substitution in danburite: Two replacements of Ca^{2+} by Sr^{2+} ($Ca^{2+} = Sr^{2+}$) and of B^{3+} by Al^{3+}, which are coupled with an incorporation of OH^- for O^{2-}: $2B^{3+} + 3O^{2-} = Al^{3+} + 3\,OH^- + \square$, are dominant in the Mexican samples. The incorporation of REE^{3+} for Ca^{2+} coupled with a simultaneous replacement of B^{3+} by Be^{2+} is present in the Vietnamese and Tanzanian samples. Different valance states of Ce are present in the Vietnamese and Tanzanian samples, leading to two different substitutions: $Ca^{2+} + B^{3+} = REE^{3+} + Be^{2+}$ and $2Ca^{2+} + 3B^{3+} = Ce^{4+} + REE^{3+} + 3Be^{2+}$, respectively.

The observed significant differences in trace element abundance not only suggest a high potential for provenance discrimination, but also provide information on the contrasting source compositions of the three deposits. The formation of danburite generally involves both metacarbonates and pegmatites as source materials. Different proportions of these two source components were involved in the formation of danburite at the three locations, and likely explain the observed trace element variations. Low REE and Be coupled with high Sr, Al, N, and OH in the Mexican samples indicate a dominant biogenic metacarbonate component, while the Vietnamese and Tanzanian samples show high REE and Be coupled with low Sr, Al, N, and OH, characteristic of a predominantly pegmatitic source. The 200- to 500-fold enrichment of LREE over HREE in the Tanzanian and Vietnamese samples results from the preferential replacement of Ca ions by similarly sized LREE ions. The negative Eu anomaly, which is characteristic of highly fractionated igneous rocks, is characteristic of Vietnamese and Tanzanian danburite and supports the predominance of the pegmatitic source at these locations.

Conflicts of Interest: The authors declare no conflict of interest.

References

1. Lindbloom, J.T.; Gibbs, G.V.; Ribbe, P.H. Crystal Structure of Hurlbutite—Comparison with Danburite and Anorthite. *Am. Mineral.* **1974**, *59*, 1267–1271.
2. Best, S.P.; Clark, R.J.H.; Hayward, C.L.; Withnall, R. Polarized single-crystal Raman spectroscopy of danburite, $CaB_2Si_2O_8$. *J. Raman Spectrosc.* **1994**, *25*, 557–563. [CrossRef]
3. Sugiyama, K.; Takéuchi, Y. Unusual thermal expansion of a B–O bond in the structure of danburite $CaB_2Si_2O_8$. *Z. Kristallogr. -Cryst. Mater.* **1985**, *173*, 293–304. [CrossRef]
4. Beran, A. OH groups in nominally anhydrous framework structures: An infrared spectroscopic investigation of danburite and labradorite. *Phys. Chem. Miner.* **1987**, *14*, 441–445. [CrossRef]
5. Hurwit, K.N. Gem Trade Lab Notes: Golden yellow danburite from Sri Lanka. *Gems Gemol.* **1986**, *22*, 47.
6. Chadwick, K.M.; Laurs, B.M. Gem News International: Yellow danburite from 346 Tanzania. *Gems Gemol.* **2008**, *44*, 169–171.
7. Huong, L.T.-T.; Otter, L.M.; Häger, T.; Ullmann, T.; Hofmeister, W.; Weis, U.; Jochum, K.P. A New Find of Danburite in the Luc Yen Mining Area, Vietnam. *Gems Gemol.* **2016**, *52*. [CrossRef]
8. De Vito, C.; Pezzotta, F.; Ferrini, V.; Aurisicchio, C. Nb–Ti–Ta oxides in the gem-mineralized and "hybrid" Anjanabonoina granitic pegmatite, central Madagascar: A record of magmatic and postmagmatic events. *Can. Mineral.* **2006**, *44*, 87–103. [CrossRef]
9. Cook, R.B. Connoisseur's: Danburite, Charcas, San Luis Potosí, Mexico. *Rocks Miner.* **2003**, *78*, 400–403. [CrossRef]
10. Hintze, J. Safari njema—AFRIKANISCHES TAGEBUCH (I): Reise zu den gelben Danburiten von Morogoro, Tansania. *Lapis Die Aktuelle Monatsschrift Fuer Liebhaber Und Sammler Von Mineralien Und* **2010**, *35*, 25.
11. Dyar, M.D.; Wiedenbeck, M.; Robertson, D.; Cross, L.R.; Delaney, J.S.; Ferguson, K.; Francis, C.A.; Grew, E.S.; Guidotti, C.V.; Hervig, R.L. Reference minerals for the microanalysis of light elements. *Geostand. Geoanal. Res.* **2001**, *25*, 441–463. [CrossRef]
12. Ottolini, L.; Cámara, F.; Hawthorne, F.C.; Stirling, J. SIMS matrix effects in the analysis of light elements in silicate minerals: Comparison with SREF and EMPA data. *Am. Mineral.* **2002**, *87*, 1477–1485. [CrossRef]
13. Balmer, W.A.; Hauzenberger, C.A.; Fritz, H.; Sutthirat, C. Marble-hosted ruby deposits of the Morogoro Region, Tanzania. *J. Afr. Earth Sci.* **2017**, *134*, 626–643. [CrossRef]
14. Möller, A.; Mezger, K.; Schenk, V. U–Pb dating of metamorphic minerals: Pan-African metamorphism and prolonged slow cooling of high pressure granulites in Tanzania, East Africa. *Precambrian Res.* **2000**, *104*, 123–146. [CrossRef]
15. Huong, L.T.-T.; Krenn, K.; Hauzenberger, C. Sassolite- and CO_2-H_2O-bearing Fluid Inclusions in Yellow Danburite from Luc Yen, Vietnam. *J. Gemmol.* **2017**, *35*, 544–550. [CrossRef]
16. Garnier, V.; Ohnenstetter, D.; Giuliani, G.; Maluski, H.; Deloule, E.; Trong, T.P.; Van, L.P.; Quang, V.H. Age and significance of ruby-bearing marble from the Red River Shear Zone, northern Vietnam. *Can. Mineral.* **2005**, *43*, 1315–1329. [CrossRef]
17. Jochum, K.P.; Stoll, B.; Weis, U.; Jacob, D.E.; Mertz-Kraus, R.; Andreae, M.O. Non-Matrix-Matched Calibration for the Multi-Element Analysis of Geological and Environmental Samples Using 200 nm Femtosecond LA-ICP-MS: A Comparison with Nanosecond Lasers. *Geostand. Geoanal. Res.* **2014**, *38*, 265–292. [CrossRef]
18. Jochum, K.P.; Stoll, B.; Herwig, K.; Willbold, M. Validation of LA-ICP-MS trace element analysis of geological glasses using a new solid-state 193 nm Nd: YAG laser and matrix-matched calibration. *J. Anal. At. Spectrome.* **2007**, *22*, 112–121. [CrossRef]
19. Jochum, K.P.; Nohl, U.; Herwig, K.; Lammel, E.; Stoll, B.; Hofmann, A.W. GeoReM: A new geochemical database for reference materials and isotopic standards. *Geostand. Geoanal. Res.* **2005**, *29*, 333–338. [CrossRef]
20. Palme, H.; Jones, A. Solar system abundances of the elements. *Treat. Geochem.* **2003**, *1*, 711.
21. Plessen, B.; Harlov, D.E.; Henry, D.; Guidotti, C.V. Ammonium loss and nitrogen isotopic fractionation in biotite as a function of metamorphic grade in metapelites from western Maine, USA. *Geochim. Cosmochim. Acta* **2010**, *74*, 4759–4771. [CrossRef]
22. Fowler, A.D.; Doig, R. The significance of europium anomalies in the REE spectra of granites and pegmatites, Mont Laurier, Quebec. *Geochim. Cosmochim. Acta* **1983**, *47*, 1131–1137. [CrossRef]

23. Braun, J.-J.; Pagel, M.; Muller, J.-P.; Bilong, P.; Michard, A.; Guillet, B. Cerium anomalies in lateritic profiles. *Geochim. Cosmochim. Acta* **1990**, *54*, 781–795. [CrossRef]

24. Takahashi, Y.; Shimizu, H.; Kagi, H.; Yoshida, H.; Usui, A.; Nomura, M. A new method for the determination of CeIII/CeIV ratios in geological materials; application for weathering, sedimentary and diagenetic processes. *Earth Planet. Sci. Lett.* **2000**, *182*, 201–207. [CrossRef]

25. Taunton, A.E.; Welch, S.A.; Banfield, J.F. Microbial controls on phosphate and lanthanide distributions during granite weathering and soil formation. *Chem. Geol.* **2000**, *169*, 371–382. [CrossRef]

26. Bao, Z.; Zhao, Z. Geochemistry of mineralization with exchangeable REY in the weathering crusts of granitic rocks in South China. *Ore Geol. Rev.* **2008**, *33*, 519–535. [CrossRef]

27. Wunder, B.; Stefanski, J.; Wirth, R.; Gottschalk, M. Al-B substitution in the system albite ($NaAlSi_3O_8$)-reedmergnerite ($NaBSi_3O_8$). *Eur. J. Mineral.* **2013**, *25*, 499–508. [CrossRef]

28. Stubican, V.; Roy, R. Boron substitution in synthetic micas and clays. *Am. Mineral.* **1962**, *47*, 1166.

29. Chen, C.; Liu, Y.; Foley, S.F.; Ducea, M.N.; He, D.; Hu, Z.; Chen, W.; Zong, K. Paleo-Asian oceanic slab under the North China craton revealed by carbonatites derived from subducted limestones. *Geology* **2016**, *44*, 1039–1042. [CrossRef]

30. Gozzi, F.; Gaeta, M.; Freda, C.; Mollo, S.; Di Rocco, T.; Marra, F.; Dallai, L.; Pack, A. Primary magmatic calcite reveals origin from crustal carbonate. *Lithos* **2014**, *190*, 191–203. [CrossRef]